Deformation induced precipitation of nano-particles in an Mg$_{88}$Co$_5$Y$_7$ alloy

Z.Z. Peng [a,b], X.H. Shao [a,*], Q.Q. Jin [a,b], C.H. Li [a,b], X.L. Ma [a,*]

[a] Shenyang National Laboratory for Materials Science, Institute of Metal Research, Chinese Academy of Sciences, 72 Wenhua Road, Shenyang 110016, China
[b] University of Chinese Academy of Sciences, Beijing 100039, China

ABSTRACT

The nano-particles precipitated along basal and non-basal dislocation lines in an Mg$_{88}$Co$_5$Y$_7$ (at.%) alloy during compression at 200 °C are observed. Aberration-corrected scanning transmission electron microscopic studies indicate that the nano-precipitate, with approximately 10 nm in diameter, has a face-centered cubic structure ($a = 0.523$ nm). The nano-precipitate and Mg matrix exhibit an orientation relationship of $(111)_{fcc}\|(0001)_{Mg}$ and $[1\bar{1}0]_{fcc}\|[2\bar{1}\bar{1}0]_{Mg}$. We propose that hot compression-induced dislocations should be responsible for activating the atomic motion of solutes and succedent precipitation. The present study indicates that segregation of supersaturated solutes along the defects should be considered in Mg alloys upon deformation at medium temperatures.

© 2016 Elsevier Ltd. All rights reserved.

1. Introduction

Solute segregation at grain boundaries are becoming increasingly attractive for improving the mechanical properties of Mg alloys, since segregation to boundaries could efficiently suppress boundary migration and then lower the grain coarsening [1–6]. This is an efficient way in weakening the strong basal texture, which tends to be developed in magnesium sheet or extrusions [1–3]. It has been documented that Gd atoms prefer to segregate or cluster at grain boundaries in Mg–Gd solid solutions after rolling and annealing [4] or dilute alloys after extrusion [5], which will be expected to suppress boundary migration. Recently, nanometer-sized Y clusters segregate to grain boundaries in Mg–Y alloys after rolling and annealing [6]. Also, periodic distribution of solute atoms along coherent twin boundaries in Mg alloys has been observed after compression and annealing, and further been proven to decrease the deformation twin growth [7]. Thus, solute atoms in Mg alloys prefer to segregate to the grain boundaries with lots of defects and to coherent twin boundaries with large lattice strain after plastic deformation.

Dislocations and stacking faults (SFs) are also defects produced during deformation, possessing local strain and tending to attract solute atoms. The solute segregating to dislocations or SFs in metallic materials was suggested long time ago [8–10]. Especially, J. D. Robson recently indicated that rare earth (RE) solutes can have a strong tendency to segregate to dislocations and inhibit their motion in RE containing wrought

Mg alloys, similar to their segregating to grain boundaries [11]. Yang et al. [12] demonstrated the occurrence of the Suzuki segregation of Zn and Y to the SFs in Mg–Zn–Y alloys after hot compression, one typical Mg alloy containing long period stacking ordered (LPSO) phase [13], using high-angle annular dark-field (HAADF) imaging technique in the scanning transmission electron microscope (STEM). However, up to now, the solute segregation to dislocations in Mg alloys is still less understood.

In the present work, we characterized the nano-particles precipitated along dislocation lines in Mg$_{88}$Co$_5$Y$_7$ alloys upon hot compression, whose dominant LPSO structures include distorted 15R, 12H, and 21R LPSO structures [14]. The microstructures and chemical features of nano-particles were investigated by the combination of HAADF-STEM and energy dispersive spectrum (EDS). The formation mechanisms of nano-particles along defects during hot compression are proposed.

Alloys with nominal composition of Mg$_{88}$Co$_5$Y$_7$ (at.%) were prepared in a high-frequency induction melting furnace under ultrahigh-purity argon, and then cooled down to the room temperature in an argon atmosphere in the furnace. A specimen with the dimensions $3.6 \times 4.6 \times 6.2$ mm^3 was cut from the ingot by low speed diamond cutting machine. Hot compression experiment was carried out at 200 °C, and a strain rate of 1.0×10^{-3} s^{-1} in an Instron-8801 fatigue machine. Prior to being compressed, the specimen was inductively heated to 200 °C at a heating rate of 5 °C s^{-1} and held for 180 s for equilibration. The compression direction was parallel to the long axis of the specimen. The specimen was deformed to failure (strain of 48%), then was immediately water quenched to room temperature for microstructure analysis. Thin foil samples for TEM were prepared by the conventional ion

milling method, a Gatan precision ion polishing system (PIPS 691) with a liquid-nitrogen-cooled stage to avoid preferential thinning effects. A Titan³™ G² 60–300 aberration-correction transmission electron microscope (TEM), equipped with a HAADF detector, energy-dispersive X-ray spectrometer systems, operated at 300 kV, was used for microstructural and compositional investigations. It is also noteworthy that the relative results of evolution of LPSO phases and intermetallic phases in $Mg_{88}Co_5Y_7$ (at.%) alloys [15] are not included in this work.

Fig. 1a shows the typical morphology of the matrix of as-cast $Mg_{88}Co_5Y_7$ alloy. There's no other precipitate phase except stacking faults (SFs) or lamellar LPSO phase, some long lines with bright contrast. These are growth SFs with Co/Y segregation on basal planes according to high-resolution Z-contrast imaging and EDS mapping, as shown in Fig. 1b–d and Fig. 1e, respectively. Fig. 1b–d are atomic resolution HAADF images of area b, c, d outlined by rectangles in (a), respectively, indicating that every long bright lines contains several growth SFs. These stacking sequence of the SFs can be described into two types: I_1 "…AB**AB′C**BCB…" and I_2 "…AB**AB′C′A**CA…", where the **B′** layer in SF I_1 and the **B′C′** layers in SF I_2 showing brighter contrast than other layers, suggesting higher concentration of Co/Y among these layers. The **AB′C** and **AB′C′A** stacking unit in SF I_1 and SF I_2 are the same as the building blocks of 15R and 18R LPSO phases in the Mg–Co–Y alloys, respectively [14]. The SFs in Mg–Co–Y alloys could be comprised of I_1, I_2, I_1 and I_2, and their corresponding twin-related variants, as denoted by "1" and "2" in Fig. 1c. Compared with the following Fig. 2, it's worthwhile to note that these growth SFs will not decompose into nano-particles in this compression process here.

Profuse nano-particles precipitated in the matrix of Mg–Co–Y sample after compression at 200 °C, coexisting with growth SFs, as presented in Fig. 2. Fig. 2a is a low-magnification bright-field TEM micrograph of the nano-particles in the matrix obtained from $[11\bar{2}0]_{Mg}$ orientation. The profuse long dark lines are parallel to basal planes, denoted by the solid arrows, with hundreds of nanometer in length and about 10 nm in width. Also, some other oblique lines show dark contrast, marked by the open arrows. Fig. 2b shows the corresponding HAADF-STEM image of Fig. 2a. Apparently, the long horizontal and oblique lines decorated with the chain-like nano-particles exhibit bright contrast, corresponding to the dark contrast in Fig. 2a. It is noteworthy that the growth SFs or lamellar LPSO phases segregated with Co/Y atoms (described in Fig. 1) can still be observed, as indicated by the arrow heads in Fig. 2b. The nano-particles are brighter than the growth SFs or LPSO phases, demonstrating the content of Y/Co in former is higher than that in latter. Thus, it indicates that the nano-particles are not produced by the decomposition of growth SFs or LPSO phases in this alloy during deformation. Fig. 2c is a low magnification HAADF image of the precipitated nano-particles taken along $[01\bar{1}0]_{Mg}$ orientation. Similarly, these nano-particles distributed parallel or slant to basal planes. The horizontal and oblique lines in Fig. 2b and c possibly represent the basal and

non-basal slip systems, since both basal and non-basal dislocations could be activated in Mg alloys during deformation at medium temperatures [16]. Then, the little difference of the angle between the oblique lines and basal planes in Fig. 2b and c should be due to the different projection of non-basal dislocations along $[11\bar{2}0]_{Mg}$ and $[01\bar{1}0]_{Mg}$ zone axis. It has been documented that the SFs and thin LPSO plates distributed in the matrix in Mg alloys may enhance the nucleation of particles along non-basal dislocations even deformed at room temperature [17,18]. Further, the sandwiched microstructure consisting of Mg layers and the SFs/thin LPSO plates would be beneficial to the activation of non-basal dislocations nucleating at their interface due to the different discontinuity of the elastic properties of Mg and SFs/thin LPSO plates [19]. Thus, this unique microstructure would increase the homogeneous nucleation of nano-particles along non-basal dislocations correspondingly. The Fig. 2d is a high magnification HAADF-STEM image of the nano-particles along the $[11-20]_{Mg}$ zone axis, suggesting that the chain-like nano-particles show homogeneous contrast, approximately or smaller than 10 nm in diameter.

The atomic arrangement of the nano-particles and orientation relationships between the phase and Mg matrix were characterized by atomic-resolution HAADF-STEM imaging and their fast Fourier transform (FFT) analysis. Atomic-resolution HAADF imaging provides a significant atomic-number-dependent contrast and the image intensity is approximately proportional to the square of the mean atomic number, Z, in the columns [20]. Fig. 3a and c show the atomic-resolution HAADF-STEM images of the nano-particles precipitated in the matrix of Mg–Co–Y alloy, taken along the zone axis of $[11\bar{2}0]_{Mg}$ and $[01\bar{1}0]_{Mg}$, respectively. The nano-particles enriched with Co/Y can be clearly distinguished since they show much brighter contrast than the matrix. In addition, the interface between the nano-particles and the matrix is fuzzy and irregular. Fig. 3b and d is the corresponding FFT images of Fig. 3a and c, respectively, where the diffraction pattern of the matrix is denoted in white and that of the nano-particle in yellow. Combining the FFT patterns and the rotation angle between Fig. 3 b and d (30°), we could calibrate that the nano-particles have a face-centered cubic (fcc) structure, with the lattice constants $a = 0.523$ nm based on the lattice parameter of the matrix ($a = 0.3209$ nm, $c = 0.5211$ nm). Moreover, the orientation relationship between the nano-particles and the matrix is derived as: $(111)_{fcc}||(0001)_{Mg}$ and $[1-10]_{fcc}//[2-1-10]_{Mg}$. The interplanar spacing of the $(\bar{1}1\bar{1})_{fcc}$ and $(0002)_{Mg}$ planes are 0.302 nm and 0.261 nm, respectively, thus the lattice misfit between the matching atomic planes can be estimated to be $\delta = \frac{d_{(0002)Mg} - d_{(\bar{1}1\bar{1})fcc}}{d_{(0002)Mg}} = 15.7\%$. Similarly, the lattice mismatch between $d_{2\bar{1}\bar{1}0}$ (0.161 nm) for Mg and d_{220}(0.185 nm) for nano-particles is 14.9%. This indicates a large lattice misfit at the interface of the nano-particles and Mg matrix, which is accommodated by some misfit dislocations, as shown by "T" in Fig. 3a and c. In addition, the misfit angles between these atomic planes are very small (<0.5°).

The chemical features of the nano-particles were further investigated by EDS analysis. Fig. 4 describes the morphology of precipitated nano-particles in the sample and their EDS mappings. It's obvious that the nano-particles are enriched with Y, deficient with Mg, but no detectable Co. This is also another proof that the nano-particles are not decomposition products of growth SFs or lamellar LPSO phases in Mg–Co–Y alloys. Furthermore, there's either no apparent O element enriched even though the compression tests were conducted at 200 °C in the atmospheric environment. The precipitation of nano-particles in the 200 °C compression Mg–Co–Y alloys is not alone. They also precipitated in the matrix after Mg–Co–Y alloys compressed at 300 °C, distributing at the recrystallized grain boundaries or within the recrystallized grains, which are not shown here.

The above examination demonstrates that the chain-like nano-particles precipitated in Mg–Co–Y alloys deformed at medium temperatures have an fcc structure ($a = 0.523$ nm), enriched with Y and no
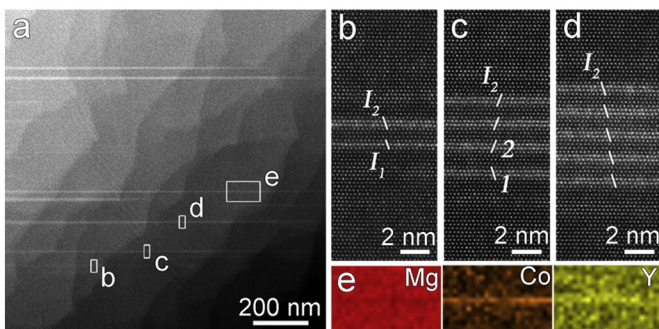

Fig. 1. (a) A low magnification HAADF-STEM image of SFs/LPSO lamellar in Mg matrix of as-cast $Mg_{88}Co_5Y_7$ alloy. (b–d) Atomic resolution HAADF images of area b, c, d outlined by rectangles in (a), respectively. (e) EDS mapping images of region e framed in (a), demonstrating the SFs/LPSO lamellar are enriched with Co/Y.
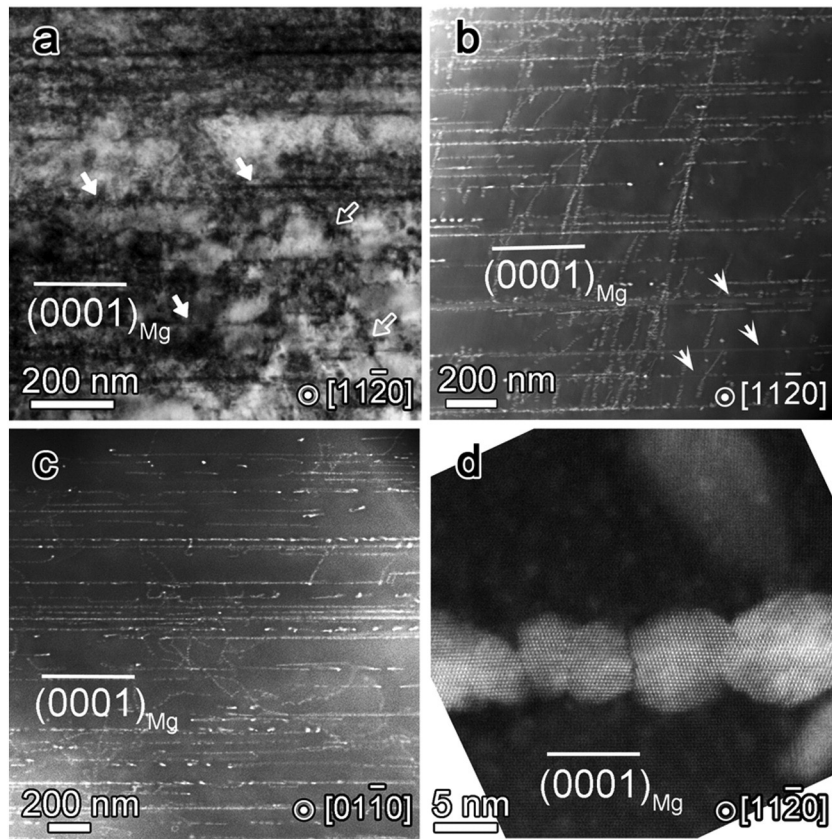
Fig. 2. Morphologies of nano-particles precipitated in Mg–Co–Y alloy during 200 °C compression process. (a) Low-magnification bright-field TEM image of the nano-particles viewed along $[11\bar{2}0]_{Mg}$ zone axis. (b) and (c) HAADF-STEM images of precipitated nano-particles obtained along $[11\bar{2}0]_{Mg}$ and $[01\bar{1}0]_{Mg}$ zone axis, respectively. This indicates the nano-particles precipitate along basal planes and non-basal planes. (d) A high magnification HAADF-STEM image of the nano-particles recorded along $[11\bar{2}0]_{Mg}$ orientation, showing the chain-like features of the nano precipitates.

detectable Co or O. The possible intermetallic phases including Mg, Co and Y elements should be Mg_3 (Co, Y) and $MgYCo_4$ considering thermodynamic assessment, in which the amount of Co elements could be obviously detected [15], hence, are ruled out here. In view of the crystallography parameters and chemical features of the nano-particles, they are possibly intermetallic compounds of Mg and Y, pure fcc Y, or yttrium hydrides. Firstly, there are three intermetallic compounds in Mg–Y binary phase diagram: $Mg_{24}Y_5$ ($I\bar{4}3m$), Mg_2Y ($P6_3$/mmc), MgY ($Pm\bar{3}m$), and one previously reported phase Mg_7Y (orthorhombic) [21]. All the crystal systems of Mg–Y intermetallics previously reported does not agree with the present result, which owns an fcc structure. There's also a possibility that the intermetallic is an isomorph of known fcc intermetallic phase, such as Mg_3Gd and Mg_2Sn. This can be easily excluded because of the uniform contrast of the phase in the atomic-resolution HAADF-STEM images shown in Fig. 3a and c.

Secondly, the precipitated nano-particles are probably pure Y with an fcc lattice. The Mg-rich part of the Mg–Y binary phase diagram indicates that the maximum solid solubility of Y in magnesium is 3.75 at.% at 566 °C (the eutectic temperature), and it decreases to 0.75 at.% at 200 °C [22]. EDS analysis indicates that the content of Y in Mg matrix of as-cast $Mg_{88}Co_5Y_7$ alloy is about 3 at.%, so in our samples Y element is supersaturated in the matrix. According to "Cottrell atmosphere" theory and Suzuki effect theory, solute atoms have a tendency to segregate to dislocation lines and stacking fault planes to lower the total energy of the alloys [9,23]. Thus, it is reasonable that the supersaturated solute Y atoms segregate to the SF planes and basal or non-basal dislocation lines when compressed the Mg–Co–Y alloy at 200 °C. It has also been reported RE elements segregating into grain boundaries are in the form of 1–2 nm clusters, with an fcc structure, in Mg–Gd alloys [4]. Meanwhile, Y can

produce structural transformation: hcp → Sm-type → double-hcp with the increase of pressure, and we could expect that Y may transform to the fcc structure at room temperature at moderately higher pressures [24]. We also calculate the lattice parameter of the most stable fcc yttrium is 0.504 nm through ab initio simulation, slightly different from the experimental result, 0.523 nm. Thus, it's possible that the nano-particles are pure Y precipitated from the supersaturated matrix to the defects in order to lower the total energy, similar to the segregation of pure Gd along the grain boundaries [4]. The basal and non-basal dislocations operated in Mg alloys during plastic deformation at moderate temperatures [16], could play an important role in the diffusion of Y to the defects. The deviation of lattice parameter from the experiments and the simulation is possibly due to the large strain between nano-precipitates and Mg matrix.

Thirdly, the nano-precipitates can be yttrium hydrides. The lattice parameters of the nano-precipitates are consistent with the parameters of yttrium hydrides (YH_2), which has an fcc structure and $a = 0.5224$ nm [25]. With more hydrogen, like YH_{2+x} ($0 < x < 1$), the parameter can be smaller [26]. RE hydrides are sometimes reported in as-cast Mg–RE alloys and are observed more frequently when the alloys are subjected to solution treatment or annealing at high temperatures [27–31]. What distinguishes the main formation mechanism is the source of hydrogen or the source of the RE elements, which are explained as follows. (i) The RE hydrides forming during melting, casting, heat treatment or sample preparation, are the reaction product of RE and hydrogen [27–30]. The source of the hydrogen can be hydrogen generated from moisture breakdown at the sample surface [27,28,30] or hydrogen previously dissolved in Mg matrix [29]. (ii) The formation of RE hydrides is probably related to the decomposition of Mg–RE intermetallic phases by hydrogen during solidification or high-temperature
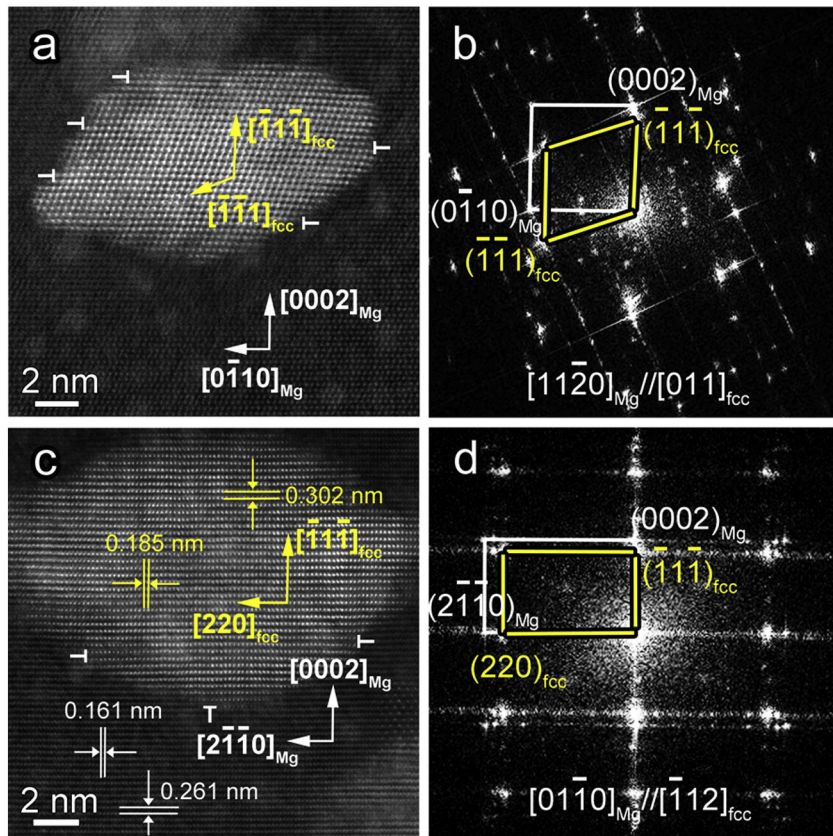
Fig. 3. Atomic structures of the nano-particles and the orientation relationships between the nano-particles and the matrix in Mg–Co–Y alloys. (a) and (c) Atomic resolution HAADF images of the nano-particles, recorded along $[11\bar{2}0]_{Mg}$ and $[01\bar{1}0]_{Mg}$, respectively, showing homogeneous contrast in a whole particle. The misfit dislocations on the interface of matrix and nano-particles are marked by "T". (b) and (d) Corresponding FFT images of (a) and (c), where the patterns of fcc precipitated phase and those of Mg matrix were marked in yellow and white, respectively. (For interpretation of the references to color in this figure legend, the reader is referred to the web version of this article.)

heat treatment [31]. Usually the reported RE hydrides are in a large size, at the micron scale and distribute inhomogeously. In our case, if the nano-precipitates along basal and non-basal dislocation lines are yttrium hydrides in Mg–Co–Y alloys, the dislocations activated during hot compression should take a significant part in the formation process. The dislocations can serve as channels for the diffusion and transportation of hydrogen from the outside environment. Then, the yttrium hydrides in the current compressed Mg alloys are probably formed as a result of reaction between supersaturated yttrium and hydrogen produced by the outside hydrides dissociation. The short deformation and reaction time should be the reason that the nano-particles are much smaller than the reported yttrium hydrides.
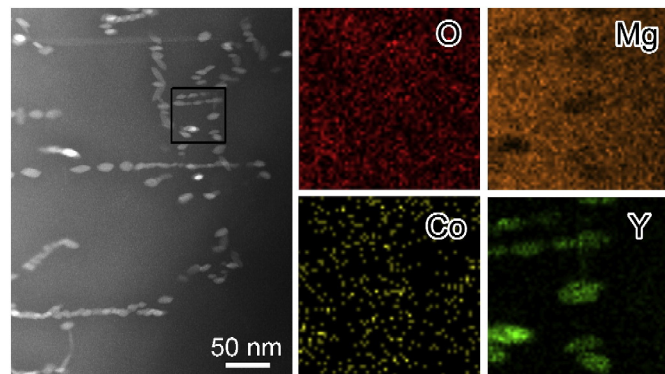
In summary, the nano-particles precipitated along dislocation lines in $Mg_{88}Co_5Y_7$ (at.%) alloy compressed at 200 °C have been studied by HAADF-STEM and EDS techniques. The nano-precipitates are about 10 nm in diameter, with an fcc structure ($a = 0.523$ nm), distributing like chains along basal and non-basal dislocation lines in the matrix. They can be pure fcc yttrium, resulting from the segregation of supersaturated Y in matrix to the defects. They also can be yttrium hydrides, which should be related to the reaction between the supersaturated yttrium and hydrogen transported from the outside. The dislocations play an important role in the formation of the nano-particles during compression. Some relevant studies are underway now.

Fig. 4. Chain-like precipitates and their EDS mapping images, indicating that the nano-particles are enriched in Y elements but no detectable Co elements.

References

[1] R.K. Mishra, A.K. Gupta, P.R. Rao, A.K. Sachdev, A.M. Kumar, A.A. Luo, Scr. Mater. 59 (2008) 562–565.
[2] N. Stanford, G. Sha, J.H. Xia, S.P. Ringer, M.R. Barnett, Scr. Mater. 65 (2011) 919–921.
[3] J.P. Hadorn, K. Hantzsche, S. Yi, J. Bohlen, D. Letzig, J.A. Wollmershauser, S.R. Agnew, Metall. Mater. Trans. A 43 (2011) 1347–1362.
[4] M. Bugnet, A. Kula, M. Niewczas, G.A. Botton, Acta Mater. 79 (2014) 66–73.
[5] J.P. Hadorn, T.T. Sasaki, T. Nakata, T. Ohkubo, S. Kamado, K. Hono, Scr. Mater. 93 (2014) 28–31.
[6] J.D. Robson, S.J. Haigh, B. Davis, D. Griffiths, Metall. Mater. Trans. A (2015).
[7] J.F. Nie, Y.M. Zhu, J.Z. Liu, X.Y. Fang, Science 340 (2013) 957–960.
[8] J.W. Cahn, Acta Mater. 5 (1957) 169–172.
[9] H. Suzuki, J. Phys. Soc. Jpn. 17 (1962) 322–325.
[10] C.C. Dollins, Acta Mater. 18 (1970) 1209–1215.
[11] J.D. Robson, Metall. Mater. Trans. A 45 (2013) 3205–3212.

[12] Z. Yang, M.F. Chisholm, G. Duscher, X. Ma, S.J. Pennycook, Acta Mater. 61 (2013) 350–359.
[13] X.H. Shao, Z.Q. Yang, X.L. Ma, Acta Mater. 58 (2010) 4760–4771.
[14] S.-B. Mi, Q.-Q. Jin, Scr. Mater. 68 (2013) 635–638.
[15] Q.-Q. Jin, S.-B. Mi, J. Alloys Compd. 582 (2014) 130–134.
[16] K. Máthis, K. Nyilas, A. Axt, I. Dragomir-Cernatescu, T. Ungár, P. Lukáč, Acta Mater. 52 (2004) 2889–2894.
[17] M. Matsuda, S. Ando, M. Nishida, Mater. Trans. 46 (2005) 361–364.
[18] J.-K. Kim, S. Sandlöbes, D. Raabe, Acta Mater. 82 (2015) 414–423.
[19] M. Tane, Y. Nagai, H. Kimizuka, K. Hagihara, Y. Kawamura, Acta Mater. 61 (2013) 6338–6351.
[20] A. Amali, P. Rez, Microsc. Microanal. 3 (1997) 28–46.
[21] M. Nishijima, K. Yubuta, K. Hiraga, Mater. Trans. 48 (2007) 84–87.
[22] J.F. Nie, Metall. Mater. Trans. A 43 (2012) 3891–3939.
[23] A.H. Cottrell, B.A. Bilby, Proc. Phys. Soc. A62 (1949) 49–61.
[24] Y. Vohra, H. Olijnik, W. Grosshans, W. Holzapfel, Phys. Rev. Lett. 47 (1981) 1065–1067.
[25] S.K. Dolukhanyan, J. Alloys Compd. 253-254 (1997) 10–12.
[26] Y. Wang, M. Chou, Phys. Rev. B 49 (1994) 10731–10734.
[27] Q. Peng, Y. Huang, J. Meng, Y. Li, K.U. Kainer, Intermetallics 19 (2011) 382–389.
[28] W. Gan, Y. Huang, L. Yang, K.U. Kainer, M. Jiang, H.-G. Brokmeier, N. Hort, J. Appl. Crystallogr. 45 (2011) 17–21.
[29] Y. Yang, L. Peng, P. Fu, B. Hu, W. Ding, J. Alloys Compd. 485 (2009) 245–248.
[30] K.Y. Zheng, J. Dong, X.Q. Zeng, W.J. Ding, Mater. Sci. Technol. 24 (2008) 320–326.
[31] S.M. Zhu, J.F. Nie, M.A. Gibson, M.A. Easton, Scr. Mater. 77 (2014) 21–24.